

Power Sharing Control for a Microgrid with PV Power Plants, Batteries and Quasi-Z-source Cascaded H-bridge Multilevel Inverter

Pablo Horrillo-Quintero¹, Pablo García-Triviño¹, Raúl Sarrias-Mena², Carlos Andrés García-Vázquez¹, Luis M. Fernández-Ramírez¹

¹ Department of Electrical Engineering

Higher Technical School of Engineering of Algeciras (ETSI Algeciras), University of Cadiz

Avda. Ramón, Puyol, s/n, 11202 Algeciras, Cádiz (Spain)

E-mail: pablo.horrillo@uca.es, pablo.garcia@uca.es, carlosandres.garcia@uca.es, luis.fernandez@uca.es

² Department of Engineering in Automation, Electronics, Computer Architecture & Networks

Higher Technical School of Engineering of Algeciras (ETSI Algeciras), University of Cadiz

Avda. Ramón Puyol, s/n, 11202 Algeciras, Cádiz (Spain)

E-mail: raul.sarrias@uca.es

Abstract. In recent years, Quasi-Z-source cascaded H-bridge multilevel inverters (qZS-CHBMLIs) have become an interesting solution for integrating renewable energy into the utility grid. The possibility of performing power conversion in a single stage, without an additional DC/DC converter, and a higher voltage gain, are their main advantages over traditional inverters. In addition, individual control of the maximum power point tracking (MPPT) can be achieved for each PV plant. Owing to the intermittent nature of PV power plants, battery energy storage systems (BESS) are commonly used to smooth out PV power fluctuations. This paper presents a control system for the active and reactive power delivered to the grid according to the system operator references and an EMS for an ES-qZS-CHBMLI. The BESS is coordinated through an energy management system (EMS) based on the state of charge (SOC). The system is evaluated under two different operation modes. One of them, where the PV power plants operate according to their MPP and the other in which the MPPT faults and thus, the PV power is decreased. A MATLAB-Simulink simulation is used to validate the proposed control system for a grid-connected single-phase configuration based on a qZS-CHBMLI with three cascade qZSI, each connected to a 4.8 kW PV power plant and a BESS.

Key words. Quasi-Z-source cascaded H-bridge multilevel inverter, PV power plant, battery energy storage system, energy management system, power control.

1. Introduction

The integration of renewable power systems into the utility grid is one of the main research challenges that need to be addressed. In addition, international commitments requirements in the energy sector are heading towards a decarbonised future. These facts have promoted the development of new solutions for the control and management of renewable energy and energy storage systems. Among the different renewable power generation technologies, PV power plants have acquired a great deal of interest in the energy generation mix [1]. In typical PV power plant topologies ([5,15] kW – [300,400] VAC) there

is a voltage source inverter (VSI) which is a buck converter, and therefore, the DC input voltage need to be greater than the peak AC output voltage. Owing to this fact, a DC/DC converter is needed to boost the PV voltage and produce the required AC voltage [2-3]. Recently, a new inverter topology based on impedance source has been proposed to replace the aforementioned configuration. The impedance source inverter (ZSI) or quasi-impedance source inverter (qZSI) are equipped with an impedance network based on inductors and capacitors which allows a higher voltage gain in comparison with the traditional VSI. The main advantage of these topologies is the suppression of the DC/DC converter, which enables the energy conversion in a single stage, boosting the DC voltage and achieving the PV power panels connected to the input to operate with MPPT. Therefore, it reduces cost and efficiency increases [4]. The employment of qZSI instead of ZSI lies in the continuous direct current obtained from the PV panels. In the case of ZSI, the current which comes from the PV panels is pulsating and difficult to measure and control [5]. The authors in [5] presented a qZSI with a battery energy system connected to the capacitor C_1 . This topology allows to balance the inverter output power for small-loads plants.

Despite the advantages of qZSI, some high-power applications, such as industrial loads, require the combination of several qZSI converters [6], which are usually known as qZS multilevel inverters (qZS-MI). Among the various topologies of qZS-MI, the cascaded H-bridge configuration (qZS-CHBMLI) is one of the most widely used because of its ease of implementation [7]. This topology can easily be scaled by adding more modules in series. The cascaded configuration allows an independent MPPT for each PV string. This topology uses four power switches in each module in single-phase systems [8].

The fluctuations of PV power generation need to be smoothed out to fulfill the grid requirements of power quality standards [9]. Usually, electrochemical batteries are a common choice for such purpose. In a qZS-CHBMLI, the BESS can be connected in parallel with a capacitor of the impedance network to build an energy storage qZS-CHBMLI (ES-qZS-CHBMLI), which adds reliability to the system against changes in solar radiation, grid demand or MPPT faults. The BESSs require an EMS to coordinate the power of each module.

In most studies [10-13], the reactive power is set to zero and the PV power plants operate at the maximum power point (MPP). To follow a reference active power (defined by the system operator) that is less than the available PV power, the PV power plants must operate out of its MPP. For reactive power, these works only considered unity power factor for reactive compensation. This paper presents a control system for the active and reactive power delivered to the grid for a microgrid based on a qZS-CHBMLI with PV power plants and BESSs and an EMS based on the SOC of the BESSs. The control system allows the PV power plants to operate in their MPPT and under a fault in the MPP strategy, maintaining the power requirements of the system operator. The proposed EMS guarantees the independent operation of the BESSs integrated into the converter, maintaining their SOC within a safe range, and limiting their maximum charge and discharge power to their rated power. The regulation of the SOC and the maximum power exchange prevents premature failure of the BES.

The rest of the paper is structured as follows: Section II describes the system under study, Section III focuses on the control system, the simulation results are discussed in Section IV, and the conclusions of the study are presented in Section V.

2. Microgrid under study

Fig. 1 shows the microgrid used in this study. It consists of three cascaded qZSI, each connected to a 4.8 kW PV power plant. The selected BESS is a lithium-ion battery. The BESS is connected in parallel to capacitor C_2 of the impedance network and a single-phase VSI is responsible for performing DC/AC conversion. The aim of the qZSI is to boost the PV voltage of each module ($V_{PV,n}$) and perform DC/AC conversion. Therefore, the VSI controls not only the AC/DC power conversion with the power flow to the grid, but also performs the MPPT voltage control of the PV power plant and the power flow exchange with the BESS. The VSI is the only controllable power converter in this configuration, which has two operating states: a) The Shoot-Through (ST) state, where two switches of the same leg are connected simultaneously, producing a short-circuit while the impedance network disconnects from the input source. The voltage boost capacity (B_n) can be derived as [11]:

$$B_n = \frac{V_{pn,n}}{V_{PV,n}} = \frac{1}{1 - 2 \cdot D_n} \quad (1)$$

where $V_{PV,n}$ is the output voltage of the PV power plant of the n -module ($n=1,2,3$), $V_{pn,n}$ is the DC input voltage to the VSI, and D_n is the ST duty ratio, which is a dimensionless parameter that relates the switching cycle (T) and the

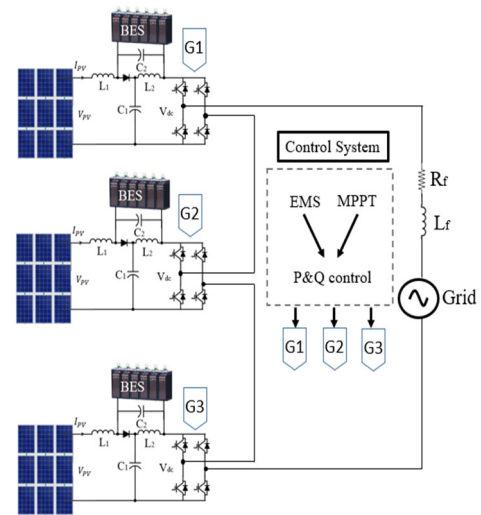


Fig. 1. Grid-connected microgrid under study with PV power plants, BESS and ES-qZS-CHBMLI.

interval of ST state (TST), and thus, the greater the TST, the higher D_n and B_n .

Likewise, the qZSI presents a non-shoot-through (NST) state, which is the typical state of the VSI. In this case, the VSI can be connected (active state) or disconnected (zero state).

The single-phase VSI has four switches in its traditional structure, with two switches connected in series per leg. Two diagonal switches are connected in the positive half-cycle, and the other two are connected in the other diagonal for the negative half-cycle. In the freewheeling mode (zero state), only the upper or lower switches are connected.

The steady state operation of the qZSI has been demonstrated in detail in the literature [12]:

$$V_{Pn,n} = \frac{V_{C1,n}}{1 - D_n} \quad (2)$$

$$i_{L1,n} = i_{L2,n} = \frac{P_{PV,n}}{V_{PV,n}} \quad (3)$$

where $V_{C1,n}$ is the voltage across the capacitor $C_{1,n}$ of the impedance network, $i_{L1,n}$ and $i_{L2,n}$ are the inductor currents of the impedance network, and $P_{PV,n}$ is the PV power.

The three cascaded qZSI must be coordinated to generate the required voltage and power. Therefore, this study considers phase-shift pulse-width-modulation (PS-PWM) based on Simple Boost Control (SBC) [14]. There are two modulating signals, phase shifted by 180° each one. This modulation compares the reference modulating signal from the control system and a triangle carrier to generate the switching signals for the positive and negative half-cycle, respectively. This modulation allows the control of the VSI, whereas the SBC modulation is applied for the ST states control. Two continuous references: V_p (upper) and V_n (lower) are defined as:

$$V_p = 1 - D \quad (4)$$

$$V_n = D - 1 \quad (5)$$

These references are limited to the maximum value of D :

$$D_{max} = 1 - M \quad (6)$$

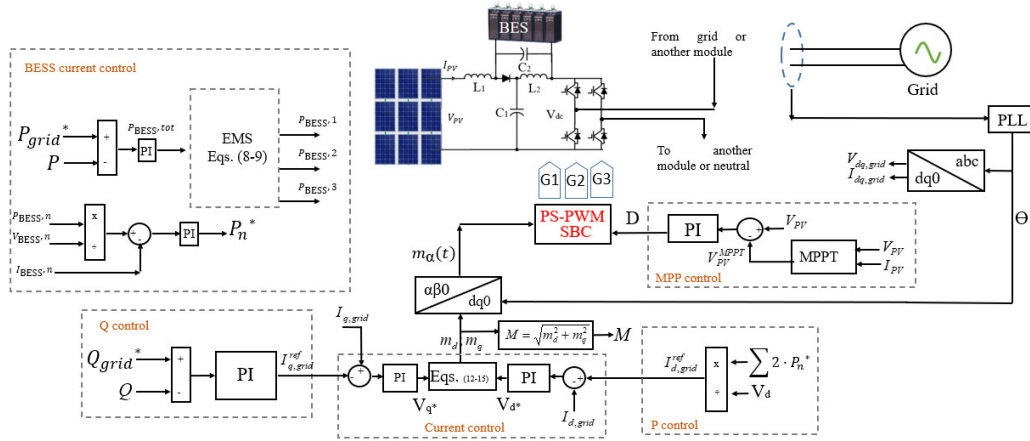


Fig. 2 Control scheme for the grid-connected microgrid under study with PV power plants, BESS and ES-qZS-CHBMLI.

where M denotes the module of the modulation index. The aforementioned modulation technique permits each H-bridge to have three different voltage levels ($+V_{Pn}$, $-V_{Pn}$, 0). In this work, seven output voltage levels are obtained according to:

$$N_{levels} = 2 \cdot c + 1 \quad (7)$$

where N_{levels} is the number of staircase levels and c is the number of H-bridge modules.

This configuration increases the output voltage, improves power quality, reduces total harmonic distortion (THD) and increases fault tolerance. To achieve a staircase multilevel output voltage, it is necessary to establish a phase shift between the carriers of contiguous modules. Typically, a phase shift of $180^\circ/c$ are applied to the triangular carriers of each module. Therefore, in this study, a phase shift of 60° is implemented, resulting in less distortion and an efficient power distribution between modules.

3. Control system

The control system consists of three independent subsystems coordinated to provide an adequate response of the system. These three subsystems are: a) MPPT control, b) EMS, and c) Power control. Fig. 2 depicts the proposed control scheme for the microgrid under study.

A. MPPT control subsystem

The MPPT control subsystem is responsible for achieving the voltage of the maximum power point (V_{mpp}) of the PV power plants. It is based on the Perturbe and Observe (P&O) algorithm. A PI controller is used to adjust the ST duty cycle (D_n) to adjust V_{pv} to V_{mpp} . Each module has its own MPPT control, which increases the reliability of the system.

B. Energy Management System

The combination of PV power plants and BESS requires a management system to achieve optimal power distribution. The aim of the designed EMS is to establish a proportional distribution of the total BESS power among the n -modules. Two restrictions are established in the proposed EMS. First, the SOCs should operate without exceeding a high threshold value, denoted as SOC_{high} and a low threshold value, denoted as SOC_{low} . In addition, the maximum power of the BESS must not exceed the rated BESS power ($P_{BESS,max} =$

$P_{BESS,rated}$). We can assume that the total PV power is the sum of each PV power plant ($P_{PV,tot} = \sum P_{PV,n}$). Hence, the system will operate in the charging mode if $P_{PV,tot} > P_{grid}^*$ and in the discharging mode if $P_{PV,tot} < P_{grid}^*$. According to [15], the discharging power of each module can be calculated as (8), where $P_{BESS,n-dis}$ denotes the BESS discharging power of each n -module, $P_{BESS,tot}$ is the total BESS power and SOC_n is the state-of-charge:

$$P_{BESS,n-dis} = \frac{P_{BESS,tot} \cdot SOC_n}{\sum SOC_n} \quad (8)$$

The charging power for each n -module can be calculated using the depth-of-discharge ($DOD_n = 1 - SOC_n$)

$$P_{BESS,n-cha} = \frac{P_{BESS,tot} \cdot DOD_n}{\sum DOD_n} \quad (9)$$

The different modes of operation are described as follows:

- Case 1: The n -modules operate in safe mode, that is, $SOC_{low} < SOC_n < SOC_{high}$. In this situation, all the BESSs operate in charging or discharging mode, and the power distribution is carried out using equations (8-9). The maximum power for each BESSs is set to its rated power, and the distribution occurs according to the SOC or DOD in each situation.
- Case 2: When $SOC_n \geq SOC_{high}$ and the system operates in a charge state, where the BESS power is set to zero, and the total BESS power is managed among the remaining n -modules according to their DOD.
- Case 3: When $SOC_n \leq SOC_{low}$ and the system operates in a discharge state, where the BESS power is set to zero, and the required power is provided by the remaining n -modules according to their SOC.

C. Power control

The power control subsystem performs a decoupled control of the active and reactive power exchanged with the grid. The control scheme is implemented out in the direct and quadrature ($d-q$) frame. For this purpose, the grid voltage and current are measured and transformed into $d-q$ components. First, the sinusoidal components are measured and transformed into the alpha-beta frame. For

a single-phase system, the quadrature component can be obtained by delaying the imaginary signal beta (β) $\frac{1}{4}$ period with respect to the real component alpha (α).

The power of each qZSI module (P_n^*) can be derived from a PI controller that adjusts the current of each BESS ($i_{BESS,n}$) to the reference BESS current ($i_{BESS,n}^*$). We can assume that the total active power that the system delivers to the grid is the sum of the individual powers of each qZSI:

$$P_{tot} = \sum P_n^* \quad (10)$$

The peak value of the grid current can be calculated from equation (11), and the injected grid current is the same for all converters owing to their series connection:

$$i_{grid}^* = \frac{2 \cdot P_{tot}}{V_{grid}} \quad (11)$$

The active power delivered to the grid (P) is controlled using the d -component of the grid current. The d -component (i_d) current control loop adjusts the d -component of the grid voltage (V_d). The $a_{n,P}$ factor defined in equation (13) distributes this voltage according to the power generation of each module. Therefore, the d -component of the modulation index M ($m_{d,n}$) for each module can be calculated as follows:

$$m_{d,n} = \frac{2 \cdot a_{n,P} \cdot V_d}{V_{pn,n}} \quad (12)$$

$$a_{n,P} = \frac{P_n^*}{P_{tot}} \quad (13)$$

where $a_{n,P}$ denotes the ratio between the active power of each module (P_n^*) and the total active power (P_{tot}).

For the reactive power control (Q), a PI controller compares the reference and measured reactive power and obtains the q -component of the grid current. Similar to the d -component control, a current control loop adjusts the q -component of the grid current (i_q) to obtain the q -component of the grid voltage (V_q). This component is also distributed among the cascaded qZSI modules according to their respective reactive power exchanges ($a_{n,Q}$). As a result, the q -component of M ($m_{q,n}$) is determined as:

$$m_{q,n} = \frac{2 \cdot a_{n,Q} \cdot V_q}{V_{pn,n} \cdot n} \quad (14)$$

$$a_{n,Q} = \frac{Q_n^*}{Q_{tot}} \quad (15)$$

where $a_{n,Q}$ denotes the ratio between the reactive power of each module (Q_n^*) and the total reactive power (Q_{tot}).

$m_{d,n}$ and $m_{q,n}$ are transformed into $m_{\alpha,n}$ and $m_{\beta,n}$, respectively. $m_{\alpha,n}$ is the desired output voltage of each cascaded qZSI module, and $m_{\beta,n}$ is the imaginary signal that can be ignored in the control system for single-phase configurations. The gate signals for the IGBTs of the qZS-CHBMLI are generated using the PS-PWM based on SBC from the shoot-through duty ratio (D_n), the α -component of M ($m_{\alpha,n}$), and the grid voltage phase angle.

4. Results and discussion

This section describes the results obtained using MATLAB-Simulink. The PV power plant is composed of three 4.8 kW,

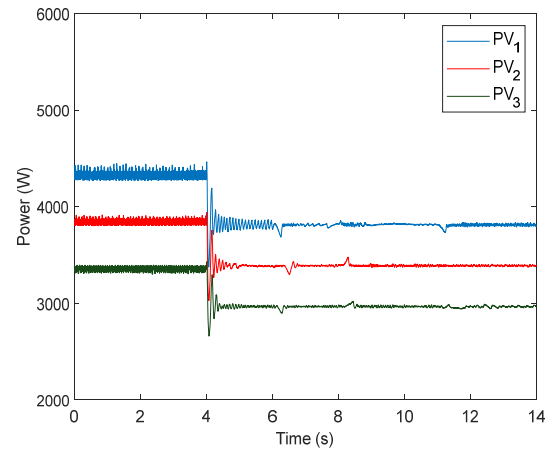


Fig. 3. Power generated by PV1, PV2, and PV3.

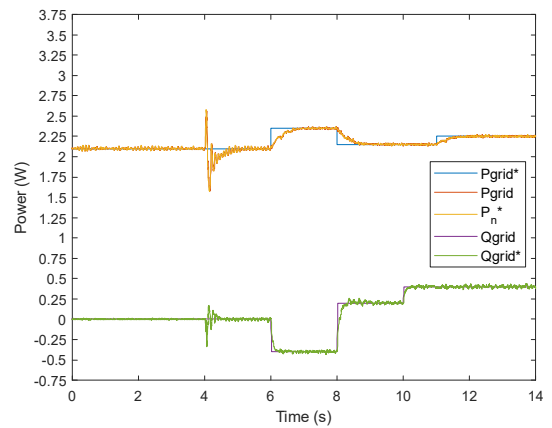


Fig. 4. Active and reactive power delivered to the grid.

with a layout of 6 modules connected in parallel and 2 in series for each PV plant. The base power of the system is selected as $P_{base} = 4.8$ kW and it is connected to a 220V single phase grid. The impedance network is formed by two inductors: $L_1 = L_2 = 0.56mH$, $R_{L1} = R_{L2} = 0.05 \Omega$, two capacitors: $C_1 = C_2 = 11mF$ and a diode. The BESS has a rated capacity of 43.63 Ah and a rated voltage of 27.5 V. The carrier frequency for the triangular signal is set to $f_c = 3.5$ kHz. The temperature of the PV modules is set at 25°C.

The irradiation for PV power plant 1 (PV1) is selected as 900 W/m², for PV power plant 2 (PV2) as 800 W/m², and for PV power plant 3 (PV3) as 700 W/m². The initial SOC_s are set to: $SOC_1 = 80\%$, $SOC_2 = 50\%$ and $SOC_3 = 20\%$. The safe conditions chosen for the BESS are as follows: $SOC_{low} = 15\%$, $SOC_{high} = 90\%$, $P_{bat,nom} = 1.2$ kW. Table 1 summarises the system operator references for active power (P_{grid}^*) and reactive power (Q_{grid}^*). Fig. 3 presents the power generated by each PV power plant

Table I. – Grid active and reactive power references.

Time (s)	P_{grid}^* (pu)	Time (s)	Q_{grid}^* (pu)
[0 – 6]	2.1	[0 – 8]	0
[6 – 8]	2.35	[6 – 8]	-0.4
[8 – 11]	2.15	[8 – 10]	0.2
[11 – 14]	2.25	[10 – 14]	0.4

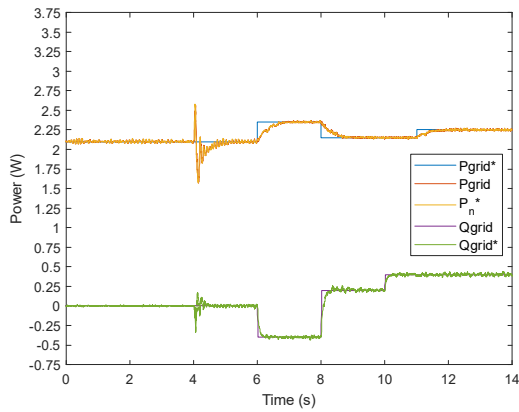


Fig. 5. Active and reactive power delivered to the grid.

during the simulation, showing the PV generation for the MPPT strategy (from 0 to 4s) and under MPPT faults (from 4 to 14s).

Fig. 4 depicts the BESSs power. When $P_{PV,tot} > P_{grid}^*$ the BESSs operate in the charging mode, and when $P_{PV,tot} < P_{grid}^*$, the BESSs operate in the discharging mode. It is remarkable that because $SOC_1 > SOC_2 > SOC_3$, $P_{BESS1} < P_{BESS2} < P_{BESS3}$ in the charging mode and $P_{BESS1} > P_{BESS2} > P_{BESS3}$ in the discharging mode. Fig. 5 depicts the active and reactive power delivered to the grid (P_{grid} and Q_{grid}) and the sum of the DC powers of each PV power plant at the input of the inverter, which is exchanged with the grid (P_n), according to the power references defined by the system operator.

The PV power plants start operating at their MPPT (from 0 to 4s) and with unity power factor ($Q_{grid}^* = 0$). According to the power balance, the BESSs are charged according to their DOD without exceeding their rated power. At 4s, the MPPT strategy faults and the EMS detects this situation. Therefore, the BESSs initiate a discharge to maintain the power references set by the system operator. At 6s, the system operator increases $P_{grid}^* = 11.28 \text{ kW}$ and the BESSs increase the discharging power to fulfill the new active power setpoint. Likewise, $Q_{grid}^* = 1.92 \text{ kVARc}$ and the power factor is set to $\cos(\phi) = 0.98$ capacitive. At 8s, Q_{grid}^* changes from a capacitive to inductive value and reaches a value of $Q_{grid}^* = 0.96 \text{ kVARi}$. In addition, P_{grid}^* reduces simultaneously its value to $P_{grid}^* = 10.32 \text{ kW}$. As

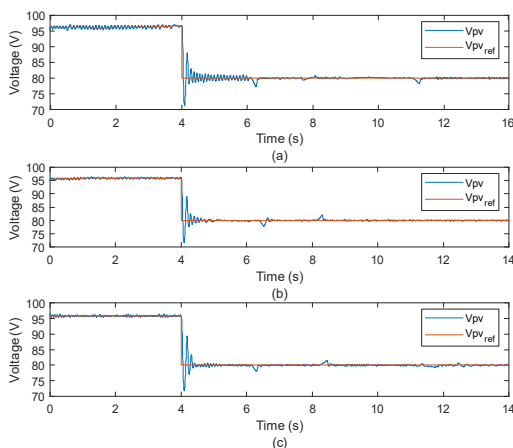


Fig. 6. PV voltage in MPP and under MPP fault: (a) PV1, (b) PV2, and (c) PV3.

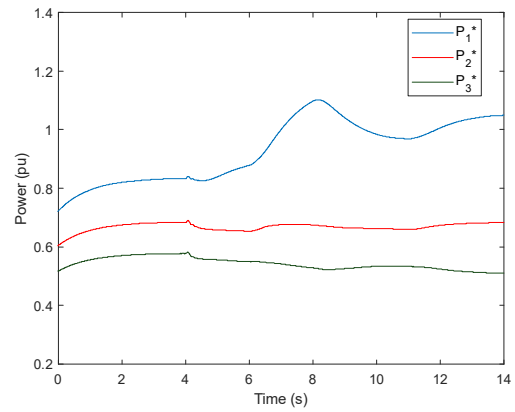


Fig. 7. DC power of each PV power plant at the input of the inverter.

shown in Fig. 3, the BESSs decrease their discharging power to balance the new active power reference. Finally, at 10s, Q_{grid}^* increases to $Q_{grid}^* = 1.92 \text{ kVARi}$ and P_{grid}^* is adjusted to $P_{grid}^* = 10.8 \text{ kW}$ at 11s. Although the MPPT strategy faults at 4s, the EMS based on the DOD proportional distribution for the charging mode and SOC for the discharging mode can balance the power control and fulfill the system operator references.

Fig. 6 shows how the MPPT subsystem can ensure that each PV module reaches its MPP voltage (V_{mpp}) from 0 to 4s. The MPPT algorithm based on P&O, reaches the voltage that guarantees the maximum power output for each irradiation situation. At 4s, the MPPT strategy fails. The PV voltage (V_{PVn}) is now limited to 80V. Therefore, the operation point of the PV power changes, and the PV power plants reduce their power.

Fig. 7 shows the DC power of each PV plant at the input of the inverter, which is exchanged with the grid (P_n). According to the irradiance and the SOC levels, each module has to provide a different level of power. As aforementioned, $SOC_1 > SOC_2 > SOC_3$ and $P_{PV1} > P_{PV2} > P_{PV3}$, thus, $P_1^* > P_2^* > P_3^*$.

Fig. 8 illustrates the SOC levels for BESS1, BESS2 and BESS3. The EMS based on SOC allows a proportional distribution for the charging and discharging modes. For the charging mode, BESS3 has the fastest dynamic owing to its low SOC ($SOC_3 = 20\%$), as shown in Fig 8c. However, as illustrates in Fig. 8a, the BESS1 has the fastest discharging dynamic owing to its high SOC

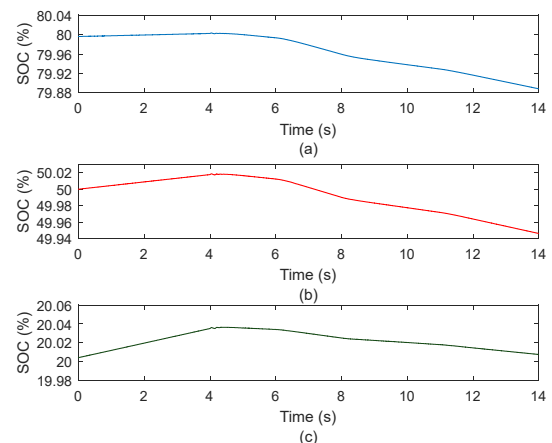


Fig. 8. BESS SOC levels: (a) BESS1, (b) BESS2, and (c) BESS3.

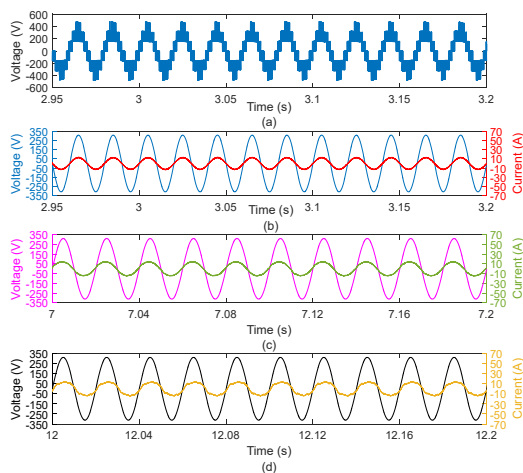


Fig. 9. (a) Seven-level output voltage of the ES-qZS-CHBMLI. (b) Grid voltage and current with unity power factor. (c) Grid voltage and current with capacitive power factor. (d) Grid voltage and current with inductive power factor.

($SOC_1 = 80\%$). Fig. 9a illustrates the seven-level staircase voltage for the ES-qZS-CHBMLI with three converters connected in series. The grid voltage and current are shown in phase in Fig. 9b due to $Q_{grid}^* = 0$. The microgrid operates with capacitive power factor ranging from 6 to 8s. Fig. 9c depicts the grid current advanced with respect to the grid voltage. In addition, as shown in Fig. 9d, the microgrid operates with inductive power factor, as the grid current is delayed with respect to the grid voltage.

The results demonstrate that the microgrid can overcome changes in the grid power references and its reliability under MPPT faults.

5. Conclusions

This work presented a new active and reactive power sharing control for a grid connected ES-qZS-CHBMLI. An EMS based on SOC proportional distribution, performs a balancing of the PV power to fulfill the system operator references. The EMS sets threshold levels for charging and discharging, as limiting the maximum BESS power to their rated power. The control scheme allows a decoupled control of the active and reactive power delivered into the grid. Two different operations modes were described. One of them, in which the PV power plants operate according their MPP and other in which MPPT strategy faults. The EMS is capable to detect the variations of PV power generation and smooth out the fluctuations. The simulations results obtained from MATLAB-Simulink shows an adequate response of the control system and the EMS. The system was tested under different irradiations conditions and grid power requirements, complying with the established references for unity, inductive and capacitive power factors.

Acknowledgement

This work was partially supported by the Regional Ministry of Economic Transformation, Industry, Knowledge and Universities of Junta de Andalucía (Grant PY20_00317) and Ministerio de Ciencia e Innovación, Agencia Estatal de Investigación, FEDER, UE (Grant PID2021-123633OB-C32 supported by MCIN/AEI/10.13039/501100011033/FEDER, UE).

References

- [1] International Renewable Energy Agency, "Global energy transformation: A roadmap to 2050," 2018. doi: 10.1057/9780230244092.
- [2] A. Cabrera-Tobar, E. Bullich-Massagué, M. Aragués-Peñalba, and O. Gomis-Bellmunt, "Topologies for large scale photovoltaic power plants," *Renew. Sustain. Energy Rev.*, vol. 59, pp. 309–319, 2016, doi: 10.1016/j.rser.2015.12.362.
- [3] Y. Liu, B. Ge, H. Abu-Rub, and F. Blaabjerg, "Single-phase Z-source/quasi-Z-source inverters and converters," *IEEE Ind. Electron. Mag.*, vol. 12, no. 2, pp. 6–23, 2018, doi: 10.1109/MIE.2018.2825479.
- [4] L. de Oliveira-Assis et al., "Simplified model of battery energy-stored quasi-Z-source inverter-based photovoltaic power plant with twofold energy management system," *Energy*, vol. 244, 2022.
- [5] B. Ge et al., "An energy-stored quasi-Z-source inverter for application to photovoltaic power system," *IEEE Trans. Ind. Electron.*, vol. 60, no. 10, pp. 4468–4481, 2013.
- [6] D. Sun, B. Ge, F. Z. Peng, A. R. Haitham, D. Bi, and Y. Liu, "A new grid-connected PV system based on cascaded H-bridge quasi-Z source inverter," *IEEE Int. Symp. Ind. Electron.*, pp. 951–956, 2012.
- [7] O. Alonso, P. Sanchis, E. Gubía, and L. Marroyo, "Cascaded H-bridge multilevel converter for grid connected photovoltaic generators with independent maximum power point tracking of each solar array," *PESC Rec. - IEEE Annu. Power Electron. Spec. Conf.*, vol. 2, pp. 731–735, 2003, doi: 10.1109/pesc.2003.1218146.
- [8] Y. Xue, B. Ge, and F. Z. Peng, "Reliability, efficiency, and cost comparisons of MW-scale photovoltaic inverters," 2012 IEEE Energy Convers. Congr. Expo. ECCE 2012, pp. 1627–1634, 2012.
- [9] W. Liang, Y. Liu, and J. Peng, "A day and night operational quasi-Z source multilevel grid-tied PV power system to achieve active and reactive power control," *IEEE Trans. Power Electron.*, vol. 36, no. 1, pp. 474–492, 2021.
- [10] Y. Li, J. Anderson, F. Z. Peng, and L. Dichen, "Quasi-ZSI for photovoltaic power generation systems," in *Conference Proceedings - IEEE Applied Power Electronics Conference and Exposition - APEC*, 2009, pp. 918–924, doi: 10.1109/APEC.2009.4802772.
- [11] S. A. Khajehoddin, A. Bakhshai, and P. Jain, "The application of the cascaded multilevel converters in grid connected photovoltaic systems," 2007 IEEE Canada Electr. Power Conf. EPC 2007, pp. 296–301, 2007, doi: 10.1109/EPC.2007.4520346.
- [12] Y. Liu, H. Abu-Rub, B. Ge, F. Blaabjerg, O. Ellabban, and P. C. Loh, *Impedance source power electronic converters*. 2016.
- [13] D. Sun, B. Ge, F. Z. Peng, A. R. Haitham, D. Bi, and Y. Liu, "A new grid-connected PV system based on cascaded H-bridge quasi-Z source inverter," *IEEE Int. Symp. Ind. Electron.*, pp. 951–956, 2012, doi: 10.1109/ISIE.2012.6237218.
- [14] J. Suganthi and M. Rajaram, "Effective analysis and comparison of Impedance Source Inverter topologies with different control strategies for Power Conditioning System," *Renew. Sustain. Energy Rev.*, vol. 51, pp. 821–829, 2015, doi: 10.1016/j.rser.2015.06.039.
- [15] P. Horrillo-Quintero, P. García-Triviño, R. Sarrias-Mena, C. A. García-Vázquez, L. M. Fernández-Ramírez, "Control System for Quasi-Z-source Cascaded H-bridge Multilevel Inverter with PV Power Generation and Battery Energy Storage System", *Proc. of the Interdisciplinary Conference on Mechanics, Computers and Electrics (ICMECE 2022)* 6-7 October 2022, Barcelona, Spain.